Shahid Ali Khan*, Muhammad Ismail, Yasir Anwar, Aliya Farooq, Bassam Oudh Al Johny, Kalsoom Akhtar, Zafar Ali Shah, Muhammad Nadeem, Mian Ahmad Raza, Abdullah M. Asiri and Sher Bahadar Khan*

A highly efficient and multifunctional biomass supporting Ag, Ni, and Cu nanoparticles through wetness impregnation for environmental remediation

https://doi.org/10.1515/gps-2018-0101
Received May 28, 2018; accepted August 30, 2018; previously published online December 4, 2018

Abstract: Plant-based materials are reported to have a wide range of applications in the environmental and biomedical sectors. In this report, we present an economic and environmentally friendly supported turmeric powder (TP) biomass for the support of Ag, Ni and Cu nanoparticles (NPs) designated as Ag@TP, Ni@TP and Cu@TP. The *in situ* syntheses of the stated NPs were achieved in aqueous medium using $NaBH_4$ as a reducing agent. The prepared NPs were applied for the degradation of *o*-nitrophenol (ONP), *m*-nitrophenol (MNP), *p*-nitrophenol (PNP), methyl orange (MO), Congo red (CR), rhodamine B (RB) and methylene blue (MB). Initially, Ag@TP, Ni@TP and Cu@TP were screened for the MO dye and antibacterial activity, where Ag@TP displayed the strongest catalytic activity for MO and bactericidal activities as compared to Ni@TP and Cu@TP. The quantity of metal ions adsorbed onto the TP was investigated by atomic absorption spectroscopy. The Ag@TP, Ni@TP and Cu@TP were characterized through X-ray diffraction (XRD), attenuated total reflectance-Fourier transform infrared (ATR-FTIR) spectroscopy, thermal gravimetric analysis (TGA), energy-dispersive X-ray spectroscopy (EDS) and field emission scanning electron microscope (FESEM) analysis.

Keywords: Ag@TP; bactericidal activity; dyes reduction; nitrophenols reduction; turmeric powder.

***Corresponding authors: Shahid Ali Khan,** Department of Chemistry, University of Swabi, Anbar-23561, Khyber Pakhtunkhwa, Pakistan; Center of Excellence for Advanced Materials Research, King Abdulaziz University, P.O. Box 80203, Jeddah 21589, Saudi Arabia; and Department of Chemistry, King Abdulaziz University, P.O. Box 80203, Jeddah 21589, Saudi Arabia, e-mail: shahidsawal007@gmail.com; and **Sher Bahadar Khan,** Department of Chemistry, King Abdulaziz University, P.O. Box 80203, Jeddah 21589, Saudi Arabia; and Center of Excellence for Advanced Materials Research, King Abdulaziz University, P.O. Box 80203, Jeddah 21589, Saudi Arabia, e-mail: sbkhan@kau.edu.sa
Muhammad Ismail: Department of Chemistry, Kohat University of Science and Technology, Kohat-26000, Khyber Pakhtunkhwa, Pakistan
Yasir Anwar and Bassam Oudh Al Johny: Department of Biological Sciences, Faculty of Science, King Abdulaziz University, P.O. Box. 80203, Jeddah 21589, Saudi Arabia
Aliya Farooq: Department of Chemistry, Shaheed Benazir Bhutto Women University, Peshawar, Khyber Pakhtunkhwa, Pakistan
Kalsoom Akhtar: Division of Nano Sciences and Department of Chemistry, EwhaWomans University, Seoul, Korea; and Department of Chemistry, King Abdulaziz University, P.O. Box 80203, Jeddah 21589, Saudi Arabia
Zafar Ali Shah: Department of Chemistry, University of Swabi, Anbar-23561, Khyber Pakhtunkhwa, Pakistan
Muhammad Nadeem: Department of Plant Protection, The University of Agriculture, Peshawar, Khyber Pakhtunkhwa, Pakistan
Mian Ahmad Raza: Department of Agriculture (Plant Breeding and Genetics), University of Swabi, Swabi, Khyber Pakhtunkhwa, Pakistan
Abdullah M. Asiri: Department of Chemistry, King Abdulaziz University, P.O. Box 80203, Jeddah 21589, Saudi Arabia; and Center of Excellence for Advanced Materials Research, King Abdulaziz University, P.O. Box 80203, Jeddah 21589, Saudi Arabia

1 Introduction

Nanoparticles (NPs) have diverse applications in drug delivery, environmental pollution control, energy, water purification and biological applications such as antibacterial, anticancer and antioxidant activities [1]. Various practices have been developed for the synthesis of NPs, such as physical, chemical and mechanical, however, most of these methods are toxic, costly, and non-ecofriendly. These methods have many other disadvantages, such as being expensive, hazard exposure like genotoxicity, carcinogenicity and cytotoxicity [2]. Therefore, there is an urgent need for the ecofriendly synthesis of NPs, which not only replace the toxic chemicals, but also proves their performance in various fields. The green synthesis of NPs might include the help of biological sources, like plants and microorganisms, which are highly appreciated not only because of their less toxic nature to human health, the environment and other organisms, but also due to their low cost, abundant nature and ease in accessibility [3, 4].

Nanoscale materials are highly fascinating in the fields of nanoscience and nanotechnology. However,

due to their high surface area to volume ratio, they are rapidly aggregated and precipitated, which largely diminishes their catalytic activities. To manage this situation, NPs are supported on various supported materials to avoid aggregation and precipitation [5, 6]. Efficient, supported materials for the stabilization of NPs are highly acknowledged in the field of catalysis that can hold and deposit NPs by their inherent structures and functional groups characteristics which provide them strong support and stability. Many types of supported materials are available in the literature such as chitosan, cellulose acetate, SiO_2, Mn_2O_3, poly(methyl methacrylate), styrene and many more [7–9]. However, recently much attention has been paid to the plant-based supported materials [10–12].

Plant-based supported materials are predominant over the conventional support because of their nontoxic nature, low cost, abundant availability, biological effectiveness, and ecofriendly nature [13, 14]. A plentiful existence, biodegradability, biocompatibility, antibacterial potential and hydrophilicity are some interesting features which give plant-based materials a distinct advantage over other supported materials [15]. Furthermore, plant-based NPs are one of the highly growing areas in the field of nanotechnology, due to their safe nature to human health and the environment.

The growth in biologically stimulated experiments for the synthesis of NPs is evolving into an important branch of nanotechnology. For instance, biosynthesized silver NPs (AgNPs) could have many applications in selective coatings for solar energy absorption, intercalation material in electrical batteries, optical receptors, chemical reactions, bio-labelling, and are largely reported as antimicrobials and anticancer agents [11, 16, 17]. Different types of plant-based NPs were produced, such as, copper, zinc, titanium [18, 19], magnesium, gold, alginate [20], and silver [21]. However, AgNPs are the most studied materials in the scientific field. In prehistoric times, silver was used to treat infectious diseases and environmental remediation [22]. In ancient times, people used silver for the treatment of burns, tract and urinary infections, chronic osteomyelitis, and central venous catheter-related infections [23]. However, with the advent of modern nanoscience and nanotechnology, the used of silver in the form of AgNPs is more beneficial. For instance, AgNPs are effectively used as antibacterial agents against various strains of bacteria, including methicillin-resistant *Escherichia coli* (*E. coli*), *Staphylococcus aureus* (*S. aureus*) and *Staphylococcus epidermidis* (*S. epidermidis*) [24, 25]. Similarly, AgNPs effectively inhibited the growth of *E. Coli* and are reported to have broad spectrum antibacterial and bactericidal potential [24]. Most importantly, AgNPs are extremely good in *in vivo* studies, as they show little toxicity to mammalian cells [26]. Plant-based NPs are efficiently used for the removal of pollutants from wastewater [27].

The literature survey revealed that a number of toxic organic and inorganic materials, and microorganisms including bacteria and viruses, are present in wastewater that comes from industrial landfills, municipal landfills and agriculture, etc. [28]. Organic pollutants are considered one of the main problematic issues in water pollution, especially nitrophenols and dyes. Several aromatic compounds such as organic dyes and nitrophenols are carcinogenic, causing nephritis, cancer, mutation and malformation [8, 29]. By viewing the toxicity of nitrophenols, the United State of Environmental Protection Agency (U.S. EPA) highlighted *p*-nitrophenol (PNP), *o*-nitrophenol (ONP), and 2,4-dinitrophenol as "priority pollutants" and restrict their concentrations in natural water to <10 ng/l (U.S. EPA, 1976). Similarly, strict rules and regulations are made mandatory for the industries to control these pollutants (U.S. EPA, 1988). The reason for the excess discharge of nitrophenols in the environment is because of their large scale applications on industrial and agriculture levels; therefore, it is extremely necessary to treat them before their exit to the environment, because nitrophenols have disturbing effects on the kidney, liver, central nervous system, and blood of both humans and animals. By contrast, dyes have considerable injurious impacts on the environment and human health. It was reported that diazo and basic dyes are the more toxic classes of dyes [30, 31]. Dyes are the noticeable hazardous pollutant, due to their mutagenicity and carcinogenicity [32]. Dyes have extremely colored materials which color the water at trace amounts and produce a thick layer on the water surface. This layer blocks the penetration of oxygen and sunlight in the water, which affects the biological phenomena of aquatic flora and fauna. Moreover, biological degradation of dyes is difficult due to the consistent nature of the microorganism. The Ecological and Toxicological Association of Dyestuff inspected 2×10^3 mg/kg LD_{50} values in 90% of about 4000 dyes. Therefore, the removal of nitrophenols and dyes from wastewater is of prime importance. Dyes are one of the most extensively studied materials because of their marketable position, toxicity and influences on the environment [9, 29]. Worldwide, approximately 10,000 dyes are commercially available and approximately 7000 tons are prepared each year by industries [33–35]. An aesthetically unfavorable percentage (10–15%) of the dyestuffs are discharged into the environment. In September 1997, the United Kingdom made an environmental

regulation that zero synthetic chemical materials were to be set free in the water, and textile industries guaranteed the treatment of waste materials [30]. Similarly, the European Community and developed countries are extremely careful in controlling dye effluents.

Synthetic dyes are the most versatile class of dyes which are used in printing, pharmaceuticals, and dyeing industries, and contribute majorly to water pollution. It is reported that color removal is usually more vital than the removal of colorless organic compounds from wastewaters, due to their hazardous effects on the aquatic life [2]. Usually, these dyes contain the aromatic moieties, which are more resistant to biological oxidation and harmful to the organism [36].

In the present study, we used turmeric powder (TP) as a supported material for silver, nickel and copper NPs for environmental applications, by reducing the nitrophenols and dyes, as well as for bactericidal potential. TP is mostly used in the coloring of food materials, medicine, and dietary supplements. The active constituent, curcumin, is present in the rhizomes, which are reported to possess cardioprotective, anti-amyloidogenic, hepato protective and hypoglycemic properties, as well as being used as antiparasitic, antifungal and antioxidant agents [37].

2 Materials and methods

2.1 Chemicals and reagents

Salts of silver, nickel and copper nitrate and sodium borohydride were purchased from Sigma-Aldrich (St. Louis, Missouri). TP was purchased from the market and nitrophenols and dyes from BDH, London, UK. The deionized water used throughout the experiment was obtained from the Millipore-Q machine present in the chemistry department of King Abdulaziz University, Saudi Arabia.

2.2 Synthesis of Ag@TP, Ni@TP and Cu@TP NPs

Stock solutions of silver, copper and nickel nitrate (1 M) were prepared, and then diluted to 0.1 M. After that, 1 g adsorbent (TP) was added to 50 ml of a 0.1 M solution. All of the solutions were kept on an orbital shaker for 5 h to completely saturate the adsorption sites, and the reactions were carried out in triplicate; the adsorption capacity was determined with an anatomic adsorption spectrophotometer. After that, the TP was dried and washed with the distilled water in order to remove any remaining unwanted materials. Then 10 mg of the dried TP was treated with 1 M of the freshly prepared $NaBH_4$ solution, where it turns black, indicating the formation of metal NPs. The synthesized NPs were then used against the reduction of isomeric nitrophenols and dyes and the bactericidal potential was evaluated.

2.3 Instrumental characterization

2.3.1 UV-visible analysis: The batch experiments were carried out using a time-dependent UV-visible spectrophotometer (Shimadzu, MultiSpec1501).

2.3.2 Fourier transform infrared analysis: Similarly, functional groups analysis and interaction of the NPs with the TP were determined through attenuated total reflectance-Fourier transform infrared (ATR-FTIR) spectroscopy using a nicolet iS50 ATR-FTIR spectrometer (Thermo Scientific).

2.3.3 Field emission scanning electron microscope and energy-dispersive X-ray spectroscopy analyses: A JEOL (JSM-7600F, Japan) system was used for confirmation of elemental analysis and for determination of the morphology and mean diameter of the prepared NPs.

2.3.4 Thermal gravimetric analysis: Stability of the materials was analyzed through thermal gravimetric analysis (TGA, Thermo Scientific TGA) in nitrogen atmosphere at 10°C/min.

2.3.5 X-ray diffraction analysis: The peak crystallinities of the NPs were scrutinized through X-ray diffraction (XRD) comprising a Cu Kα radiation ($\lambda = 0.154$ nm) source of a Thermo Scientific diffractometer. A field emission scanning electron microscope (FESEM) (JSM-7600F, JEOL, Japan), was used for the surface morphology.

2.3.6 Atomic adsorption study: The uptake of the Ag, Cu and Ni ions by TP was studied using a PerkinElmer 400 flame atomic absorption spectrophotometer. After 5 h, the TP adsorbed metal ions were collected and filtered using Whatman No. 42 filter paper.

2.4 Reduction of nitroarene and azo dyes

A concentration of 0.1 mmol PNP and 0.05 mmol of all the dyes, along with freshly prepared $NaBH_4$ (1 M) were used in this experiment. By adding $NaBH_4$, the nitrophenols shifted and increased in wavelength (red shift) due to the formation of more stable phenolate anions, which appeared at 400 nm, however, the azo dyes transformed to the hydrazine derivative and cationic dyes transformed to leuco derivatives after $NaBH_4$ addition. The modified TP (after adsorbing the metal ions) becomes black in color after treating with 0.5 ml of 1 M freshly prepared $NaBH_4$ solution. The black color clearly shows the formation of metallic NPs on the surface of TP. The synthesized NPs were dried and applied for the degradation of isomeric nitrophenols and dyes. Before the addition of NPs, 0.5 ml of 1 M freshly prepared $NaBH_4$ solution was added to a UV cuvette individually containing 3 ml of nitrophenols and dyes solution. The decrease in the concentration of the analyte was measured with UV-vis spectrophotometer.

2.5 Bacterial cell culturing

Escherichia coli O157:H7 was used as a model for evaluation of the antibacterial activities, and was supplied by King Fahad Hospital,

Jeddah. For the antibacterial test, bacterial cells were grown on nutrient agar (Sigma-Aldrich-70148) comprising 1 g/l meat extract, 2 g/l yeast extract, 2 g/l sodium chloride, 5 g/l peptones, and 15 g/l agar in distilled water. Medium plates of nutrient agar were prepared, solidified and sterilized. Bacterial cultures were cleaned through solidification on these plates.

2.6 Antibacterial assessment

The colony forming units count method was used for the assessment of antimicrobial activities of the synthesized materials. About 0.15 g/ml of samples that contained 9 ml of liquid medium (Nutrient Broth) was added to all test tubes. Afterwards, 1 ml of *E. coli* O157:H7 was put in a 9 ml tube that contained liquid medium and incubated at 37°C for 24 h. The samples were diluted serially and later spread on nutrient agar. Using a colony counter, the number of colonies were counted and the experiment was performed in triplicate.

3 Results and discussion

3.1 Synthesis and characterization

The percent adsorption of metal ions by TP was calculated by the decrease in the concentration of Cu^{2+}, Ag^{1+} and Ni^{2+} ions. The decreases in metal ion concentrations from their solution were calculated by comparison with their corresponding stock solution using Eq. (1):

$$\text{Percent metal ions uptake} = \frac{(Cs - Ct) \times 100}{Cs} \quad (1)$$

where Cs is the concentration of metal ions (mg/l) and Ct is the residual metal ions concentration after 5 h of treatment with TP.

The percent adsorptions of the Cu^{2+} ions were highest among all the salts, which showed 44.26% adsorption capacity as compared to Ni^{2+} and Ag^{1+}, which were 41.67% and 37.49%, respectively.

The uptake of the metal salts is due to the interactions with -OH functional groups present in the chemical constituents of the TP, largely phenolic and terpenoids compounds. The % adsorption of metal ions are presented in Table 1.

Similarly, the concentrations of metal ions in the solution were calculated by using Eq. (2):

$$\text{Conc of metal ions in reaction mixture (Cr)} = \frac{(Cs \times 50)}{1000} \quad (2)$$

were Cr is the atomic adsorption reading, 50 is the amount of sample taken for adsorption from 1000 ml stock solution containing 1 g of adsorbent, and Cs is the concentration of metal ions in the stock.

The amounts of metal ions adsorbed on 1 g of adsorbent from the stock solution were calculated by using Eq. (3):

$$\text{Amount of metal reduced} = \frac{(Cr \times Pa)}{50} \quad (3)$$

Cr is the concentration of metal ions in the mixture and Pa is the percent of metal ions adsorbed on 1 g of adsorbent, as shown in Figure 1A.

The amounts of the metal adsorbed by TP were calculated using Eq. (3). The amounts of Ag^{1+}, Cu^{2+} and Ni^{2+} adsorbed in 1 g of TP were 113.4 mg, 96.26 mg and 65.21 mg, respectively, as shown in Figure 1B.

Figure 2A depicts the diffraction pattern of TP and NPs. A broad peak at $2\theta = 20°$ appeared in the XRD data of all samples, due to the presence of organic constituents present in the TP and NPs. The Ag@TP displayed diffraction peaks at $2\theta = 38.33°$ (111), $2\theta = 64.7°$ (220) and $2\theta = 77.7$ (311) [38, 39]. The Cu@TP NPs displayed a sharp peak at $2\theta = 43.1°$ (111). The Ni@TP displayed peaks at $2\theta = 43.6°$ (111), and $2\theta = 48.8°$ (200) [40, 41].

The functional groups and particle interactions with the materials were determined using ATR-FTIR. All of the samples indicated a broad peak at approximately 3390 cm^{-1} which is assigned to the -OH stretching vibration. The broadness of the peak indicates the presence of H-bonding, which was clearly found in all the stated samples. Similarly, another common peak in all of the NPs, including TP, is the C-H asymmetric stretching

Table 1: Atomic adsorption study adsorption potential of turmeric powder.

Serial number	Sample	% Adsorption of Cu^{2+} ions	% Adsorption of Ag^{1+} ions	% Adsorption of Ni^{2+} ions
1	C_0	35.12	32.09	40.51
2	C_f	7.28	12.60	11.65
3	% Adsorption	79.27%	60.73%	71.24%

C_o is the initial concentration and C_f is the final concentration of the metal salts after treating with turmeric powder.

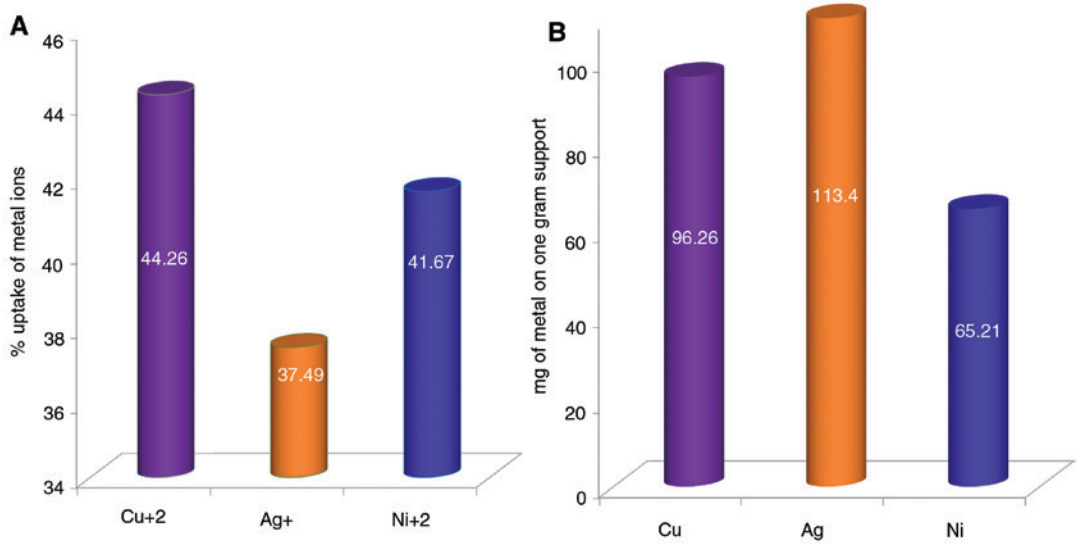

Figure 1: Atomic adsorption studies for the percent uptake of different metal ions by turmeric powder (TP) (A); mg of metal ions adsorbed on 1 g of the adsorbent (B).

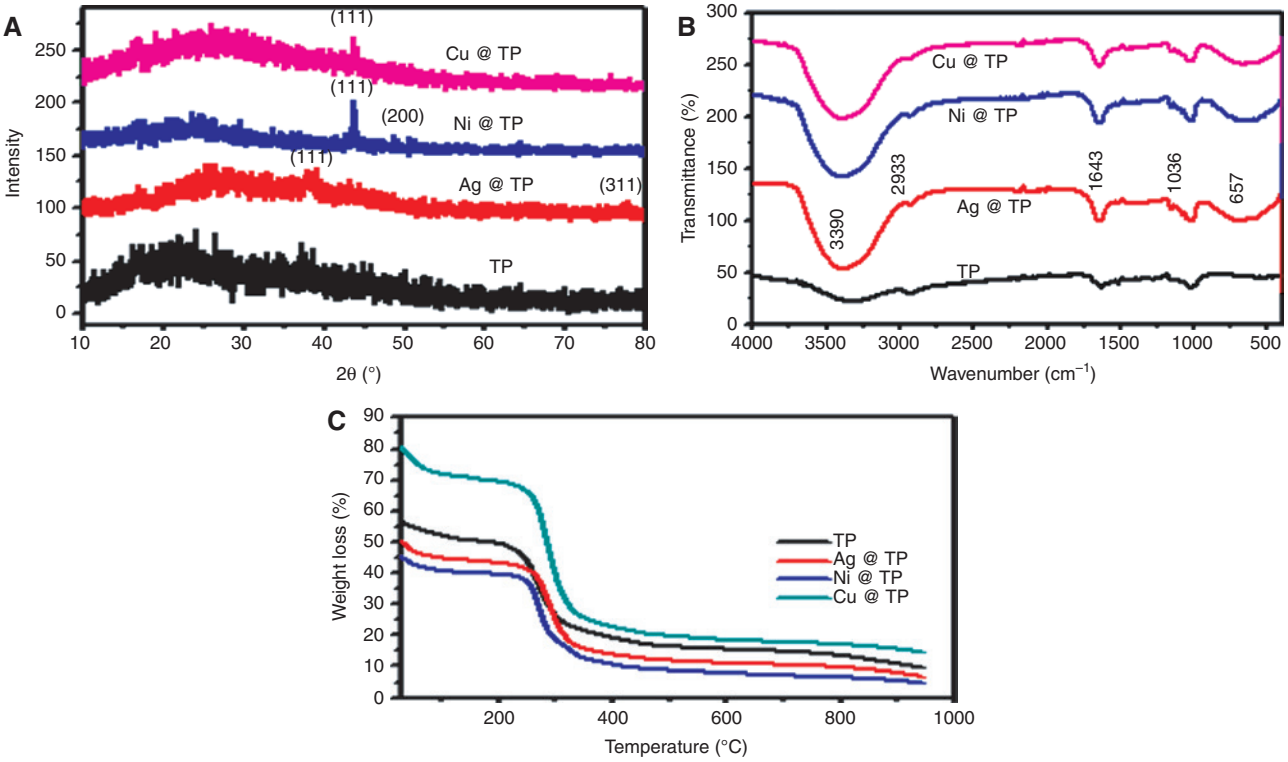

Figure 2: (A) X-ray diffraction (XRD), (B) Fourier transform infrared (FTIR) and (C) thermal gravimetric analysis (TGA) spectrum of pure turmeric powder (TP), Ag@T, Ni@T and Cu@T nanoparticles (NPs).

vibration, which appeared at 2933 cm^{-1}; this is because the organic compound contains C-H bonds. All of the samples also contain a peak at 1643 cm^{-1}, which might be due to the presence of a conjugated carbonyl group. This group is present in the TP, which mainly contains curcumin and curcuminoids with conjugated carbonyl groups. The absorption peaks at 1036 cm^{-1} in all of the samples are due to the C-O vibrations. The metal NPs peaks were clearly displayed at 657 cm^{-1} in Ag@TP, Ni@TP and Cu@TP NPs. No change in the chemical composition of TP was observed, which suggested that TP acts only as support to the NPs. The FIR-ATR data are depicted in Figure 2A.

TGA was performed to explore the stability of NPs. The TGA thermogram of the stated NPs displayed two weight losses. The first weight loss which occurred at 246°C is due to the TP, while the second weight loss, which occurred at 335°C, is attributed to the presence of the uptake metal ions as shown in Figure 2C.

The FESEM images were taken at low and high resolutions. The FESEM images of the pure TP were recorded at 10 µm and 100 nm, and showed a highly rough increase surface of the TP, while the Ag@TP NPs at 100 nm which displayed 15–20 nm particle size are supported on the surface of the TP, as well as adsorbed inside the TP as shown in the inset of Figure 3C and D.

The energy-dispersive X-ray spectroscopy (EDS) spectrum is depicted in Figure 4. The EDS spectrum showed that the NPs are supported by the plant materials and give a strong peak at 3 KeV, which confirms the formation of AgNPs [42]. The C, O and Ag appeared in the EDS spectrum at 65.02 weight%, 24.78 weight% and 10.20 weight%, respectively. The presence of C and O elements in the EDS spectrum supported the stabilization of Ag NPs by the TP.

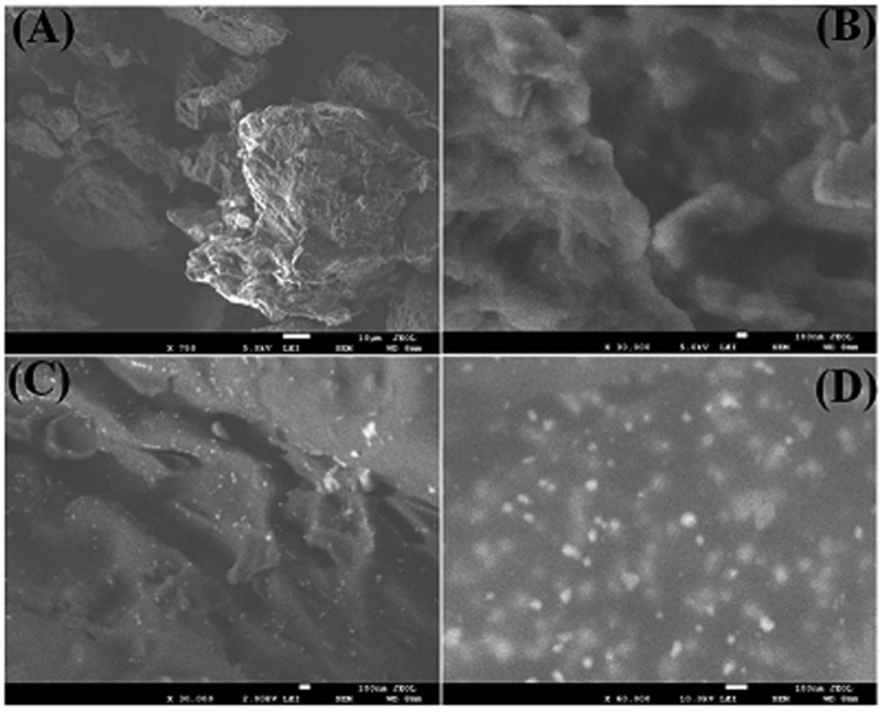

Figure 3: (A) Low and (B) high resolution field emission scanning electron microscope (FESEM) spectrums of turmeric powder (TP) and (C, D) high resolution spectrum of Ag@T nanoparticles; the white spot in the spectrum clearly indicated the presence of Ag nanoparticles.

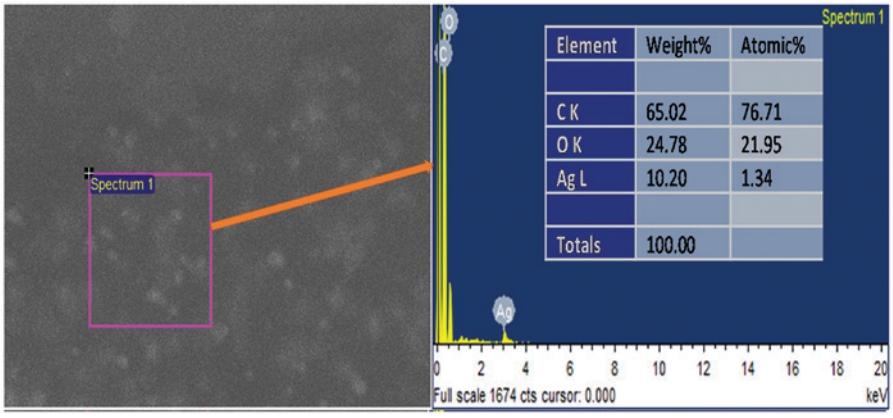

Figure 4: Energy-dispersive X-ray spectroscopy (EDS) spectrum of Ag@TP nanoparticles.

3.2 Catalytic reduction of nitrophenol

Initially, the TP and its adsorbed Ag, Ni and Cu ions were evaluated for their adsorption capacity. Some 10 mg of the pure TP and the modified TP were used against 3 ml of 0.05 mmol methyl orange (MO) solution for the adsorption or degradation phenomena. However, we observed no such physical or chemical change after 4 h, which showed that the materials were inactive for adsorption or degradation. After this, 10 mg of the TP and TP adsorbed Ag, Ni and Cu ions were treated with 0.3 ml of 1 M aqueous $NaBH_4$ solution, which imparts a black color to the adsorbed metal ions on TP, suggesting the formation of the respective metal NPs; however, the pure TP was not changed. We observed that the TP is not reduced to NPs after the addition of $NaBH_4$, which reflects that the pure sample has no inherent properties for NPs formation, and it is only the adsorbed metal ions, chelated with the TP, which are reduced to metallic NPs after treating with the reducing agent.

After the formation of metal NPs, the catalysts were screened against 3 ml of 0.05 mmol solution of MO dyes; the fastest catalytic performance was achieved with Ag@TP NPs followed by Cu@TP, and the slowest performance was obtained with Ni@TP, while the TP had no role in this reduction reaction, as shown in the inset of Figure 5A. After screening the catalysts, the Ag@TP catalyst was largely studied for the reduction of isomeric nitrophenols (ONP, MNP and PNP), two cationic dyes (methylene blue [MB] and rhodamine B [RB]) and two anionic dyes (MO and Congo red [CR]).

Some 10 mg of the Ag@TP NPs was employed for the reduction of 3 ml of 0.1 mmol of ONP and MNP and PNP and monitored in a time-dependent UV-visible spectrophotometer. The phenolate anions of ONP and MNP were exhibited at 415 nm and 395 nm and 400 nm respectively, and gradually decreased with the passage of time, as shown in Figure 5B and C. The conversion of PNP to *p*-aminophenol (PAP) is a benchmark reaction to check the catalytic activity of a catalyst, because it is a green and atom-economic reaction, where all the reactants are completely converted into the desired product without any side reactions. Furthermore, PAP is an extremely important class of organic compounds, which are mainly used at the industrial level for the development of hair color, photographic developer, and dye production [43]. The pure PNP exhibited a peak at λ_{max} 318 nm, however, after addition of the reducing agent ($NaBH_4$), the PNP shifted to a red shift at λ_{max} 400 nm. This is because the reducing agent takes the proton from the OH group of phenol, thereby creating a phenolate anion. The phenolate anion of PNP is more

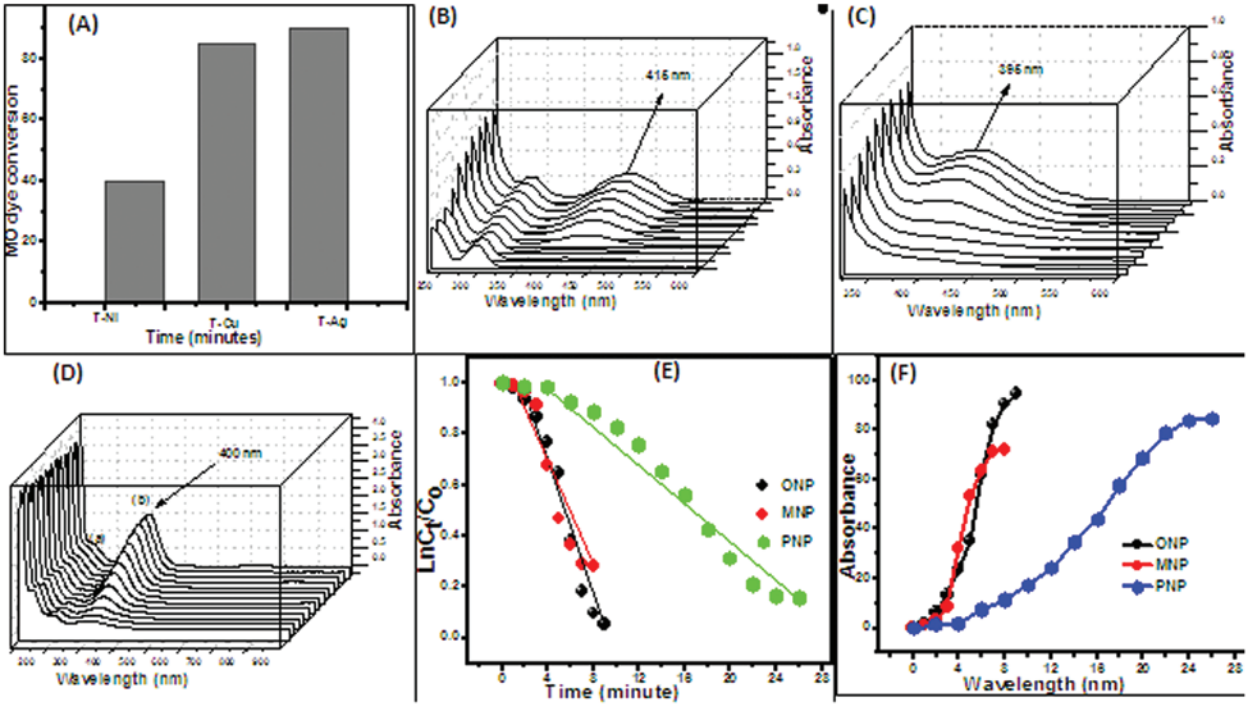

Figure 5: Comparing the Ag@TP, Ni@TP and Cu@TP for methyl orange (MO) reduction (A), time-dependent UV-vis spectrum for the reduction of *o*-nitrophenol (ONP) (B), *m*-nitrophenol (MNP) (C) and *p*-nitrophenol (PNP) (D) to aminophenol, rate of reaction deduced from lnCt/Co *vs* time (E) percent reduction of the isomeric nitrophenols (F). The points a, and b in the spectrum (D) indicate the *p*-aminophenol peak and phenolate anion.

stable than the pure PNP due to the negative charge on the oxygen atom. The oxygen atom itself is highly electronegative, thus efficiently delocalizing the electrons onto the benzene ring, which is why the phenolate anions move toward the red shift (longer wavelength). Briefly, during this hydrogenation reaction, 10 mg of the Ag@TP NPs was employed for the reduction of 3 ml of 0.1 mmol PNP to PAP and monitored using the time-dependent UV-visible spectrophotometer, as shown in Figure 5D. The phenolate anions gradually decreased at 400 nm, labelled as point (b) in the inset of Figure 5D, and a gradual increase was observed at approximately 290 nm. The peak observed at 290 nm is largely reported in the literature for PAP, labelled as point (a) in the inset of Figure 5D. The % reductions are shown in the inset of Figure 5F, where 95% of ONP is converted in 9 min and 72% of MNP in 8 min, while 85% of PNP is converted in 26 min. The linear fit plots are depicted in Figure 5E, which show 0.935, 0.926 and 0.955 R values for ONP, MNP and PNP, respectively.

3.3 Catalytic reduction of methyl orange

Dyes are an extremely important class of organic compounds which are largely used in the textile industries, and it is believed that the dye industries played a key role in the development of a country [44]. However, unfortunately, the dye industries dump their remaining dyes to the water resources, which pollute the water and even at trace amounts, the dyes colorize the water and produce a thick foam-like layer on the surface of water which stops the diffusivity of sunlight and oxygen, thus creating a huge problem for aquatic flora and fauna and affecting the environment. Therefore, the complete eradication of dyestuff from the environment is extremely important. In the present study, we applied the synthesized Ag@TP NPs for the reduction of two anionic and two cationic dyes. Some 3.5 ml of the solution containing 3 ml of 0.05 mmol of the respective dyes and 0.5 ml of 1 M $NaBH_4$ solutions were placed in a cuvette and 10 mg of the Ag@TP NPs were added to the cuvette. MO dyes have λ_{max} at ~464 nm and CR at ~500 nm. After the addition of $NaBH_4$ solution, both dyes are converted to hydrazine derivatives [45, 46]. The reduction reactions started after the addition of the catalyst, and then periodically investigated through the time-dependent UV-vis spectrophotometer, as shown in Figure 6A and B. During the course of the reaction, 90% of MO was converted in 13 min and approximately 94% of CR dye was reduced in 26 min, as depicted in Figure 6A and B. The kinetics for the Ct/Co

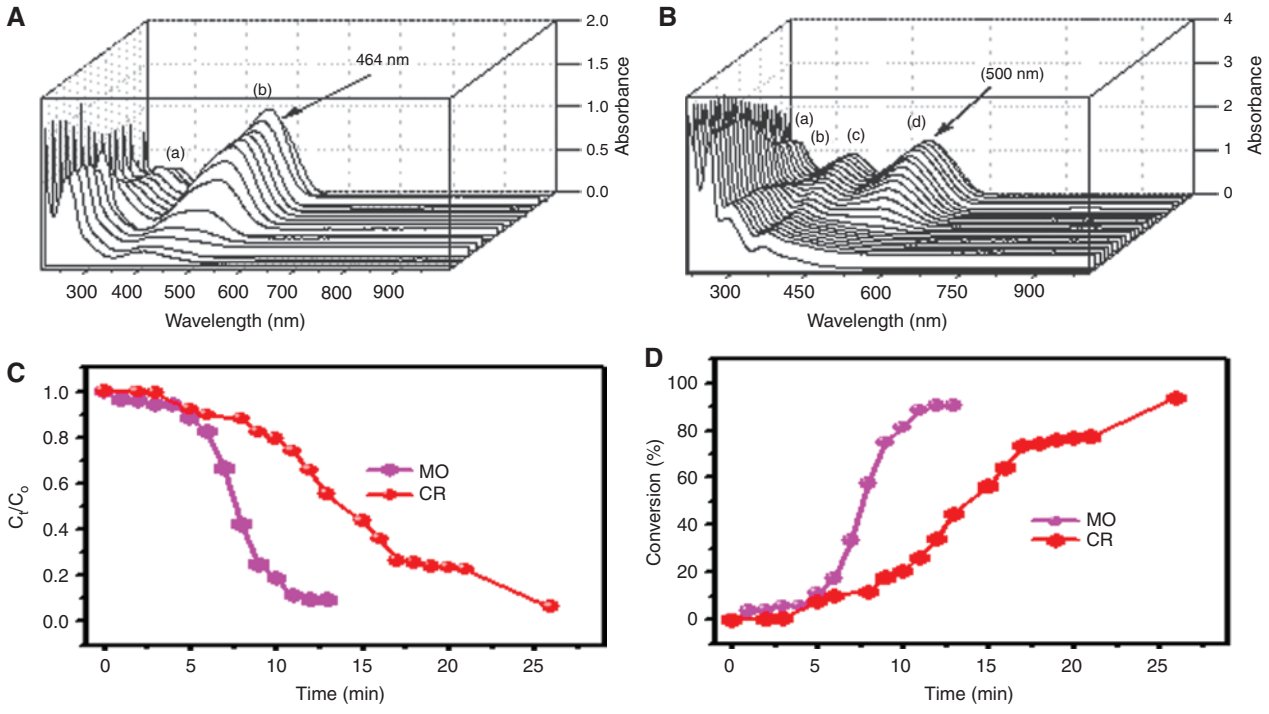

Figure 6: Time-dependent UV-vis spectrum for the degradation of (A) methyl orange (MO), (B) Congo red (CR); the points a and b in the spectrum of MO indicate the -NH2 and MO hydrazine derivatives and points a–d in the spectrum of CR are due to -NH2, naphthalene and hydrazine derivative of CR, respectively. The kinetics due to the decrease in the original concentration with respect to time appeared in (C) and % reduction of dyes (D).

and % reduction of the dyes are depicted in Figure 6C and D, respectively.

Keeping the same experimental conditions of the cationic dyes, 3.5 ml of solution containing 3 ml of 0.05 mmol MB and RB dyes and 0.5 ml of 1 M $NaBH_4$ solution were placed in a cuvette along with 10 mg of the Ag@TP NPs. The MB dyes appeared at $\lambda_{max} \sim 664$ nm and RB appeared at 554 nm, which gradually decreased with the passage of time, as depicted in the inset of Figure 7A and B. After the addition of $NaBH_4$ solutions, both the cationic dyes, MB and RB, are converted to leuco MB and leuco RB. The kinetics of the cationic dyes are displayed in Figure 7C and D, respectively. Approximately 99% of MB and RB dyes are reduced in 11 min and 18 min, respectively.

3.4 Antibacterial activity

The synthesized NPs were evaluated for antibacterial activity. All the mentioned NPs exhibited a stronger performance then pure TP. Figure 8 and Table 2 show the development properties of the cell viability of *E. coli*

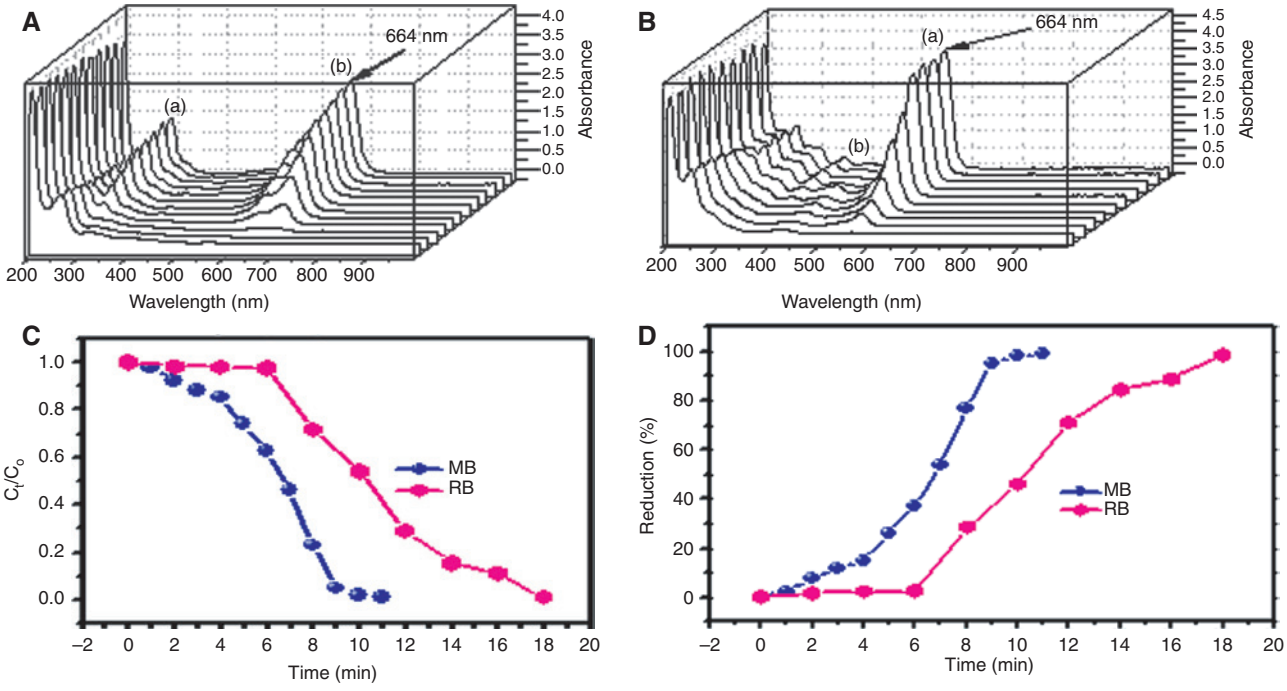

Figure 7: Time-dependent UV-vis spectrum for the reduction of (A) methylene blue (MB) and (B) rhodamine B (RB); the points a and b in the spectra of MB and RB indicate the -NH2 and MB luco derivatives. The kinetics due to the decrease in the original concentration with respect to time appeared in (C) and % reduction of dyes (D).

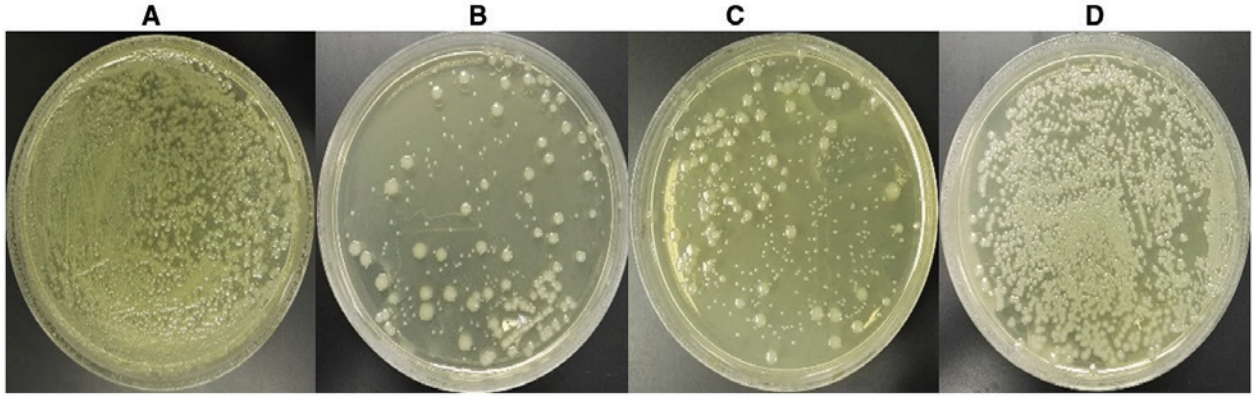

Figure 8: Nutrient agar plates showing antibacterial potential of (A) turmeric powder (TP), (B) Ag@TP, (C) Ni@TP and (D) Cu@TP. Ag@TP indicated the strongest antibacterial activity, while the nanoparticles (NPs) showed good activity, then turmeric powder (TP).

Table 2: The growth characteristics of *Escherichia coli* in the presence of the synthesized catalyst.

Samples	Incubation time (h)	(cfu/ml)	% Reduction
TP	12	125×10^5	0
TP	24	123×10^5	1
Ag@TP	12	78×10^5	47
Ag@TP	24	47×10^5	72
Ni@TP	12	83×10^5	42
Ni@TP	24	52×10^5	67
Cu@TP	12	105×10^5	10
Cu@TP	24	86×10^5	44

(O157:H7) after treatment with TP, Ag@TP, Ni@TP and Cu@TP. The results identify that TP, after 12 h and 24 h, does not exhibit development prevention against *E. coli*. It was seen that Ag@TP, Ni@TP and Cu@TP exhibited improved prevention activity against the designated pathogenic bacteria. However, Ag@TP NPs indicated the greatest prevention rate with *E. coli*. Since *E. coli* is a gram-negative bacteria containing a thin peptidoglycan layer and has a complex cell wall, comprised of two cell membranes [47]. The cell membrane is negatively charged, which may work together with the positively charged Ag@TP NPs. The permeability of cell membranes is changed due to the interaction of Ag@TP NPs which stopped the intake of nutrients into the cell. Apart from the procedure, these NPs can also develop species that are highly reactive, such as hydrogen peroxide, superoxides or hydrogen radicles. For this reason, the feasibility and development of these pathogenic bacteria is reduced by using the stated NPs as compared with TP. This results clearly demonstrate that Ag@TP NPs can reduce the organic pollutant effect as well the growth of *E. coli*, which reflects their applications in the environmental and biological sectors.

4 Conclusion

In the present study we report the facile and green synthesis of Ag, Ni and Cu NPs supported on the pure TP. The adsorption capacities of the turmeric plant were determined using a flame atomic adsorption spectrophotometer. The synthesized Ag@TP, Ni@TP and Cu@TP NPs were evaluated for their potential in isomeric nitrophenols and dyes reduction, where Ag@TP NPs indicated the strongest catalytic activity. The synthesized NPs were also evaluated against the gram-negative *E. coli*, where the Ag@TP NPs indicated the highest activity as compared to Ni@TP and Cu@TP NPs. The Ag@TP NPs are adsorbed on the surface and inside the surface of TP, which gives a high stability to Ag@TP NPs; this makes these catalysts suitable for environmental and biological studies.

Acknowledgments: The authors highly acknowledge the Center of Excellence for Advanced Materials Research, King Abdulaziz University, Jeddah, Saudi Arabia.

Conflict of interest statement: The authors declare no conflict of interest regarding this article.

Statement regarding human and animal rights: This article does not contain any research with human or animal subjects performed by any of the authors.

References

[1] Gittins DI, Bethell D, Schiffrin DJ, Nichols RJ. *Nature* 2000, 408, 67.
[2] Khan SA, Khan SB, Kamal T, Yasir M, Asiri AM. *Int. J. Biol. Macromol.* 2016, 91, 744–751.
[3] Ismail M, Gul S, Khan MI, Khan MA, Asiri AM, Khan SB. *Green Process. Synth.* 2019, 8, 118–127.
[4] Rai M, Yadav A, Gade A. *Biotechnol. Adv.* 2009, 27, 76–83.
[5] Khan SB, Khan SA, Marwani HM, Bakhsh EM, Anwar Y, Kamal T, Asiri AM, Akhtar K. *RSC Adv.* 2016, 6, 110077–110090.
[6] Gul S, Rehan ZA, Khan SA, Akhtar K, Khan MA, Khan M, Rashid MI, Asiri AM, Khan SB. *J. Mol. Liq.* 2017, 230, 616–624.
[7] Khan SA, Khan SB, Asiri AM. *RSC Adv.* 2016, 6, 83196–83208.
[8] Astruc D, Lu F, Aranzaes JR. *Angew. Chem. Int. Ed.* 2005, 44, 7852–7872.
[9] Khan SA, Khan SB, Asiri AM. *Sci. Rep.* 6, 35107, 2016.
[10] Dubey SP, Lahtinen M, Sillanpää M. *Process Biochem.* 2010, 45, 1065–1071.
[11] Nadagouda MN, Iyanna N, Lalley J, Han C, Dionysiou DD, Varma RS. *ACS Sustain. Chem. Eng.* 2014, 2, 1717–1723.
[12] Ismail M, Khan MI, Khan SB, Khan MA, Akhtar K, Asiri AM. *J. Mol. Liq.* 2018, 260, 78–91.
[13] Bello BA, Khan SA, Khan JA, Syed FQ, Mirza MB, Shah L, Khan SB. *Biochem. Biophys. Res. Commun.* 2017, 490, 889–894.
[14] Samadi N, Golkaran D, Eslamifar A, Jamalifar H, Fazeli MR, Mohseni FA. *J. Biomed. Nanotechnol.* 2009, 5, 247–253.
[15] Krishnaraj C, Jagan E, Rajasekar S, Selvakumar P, Kalaichelvan P, Mohan N. *Colloids Surf. B.* 2010, 76, 50–56.
[16] Bello BA, Khan SA, Khan JA, Syed FQ, Anwar Y, Khan SB. *J. Photochem. Photobiol. B: Biol.* 2018, 175, 99–108.
[17] McFarland AD, Van Duyne RP. *Nano Lett.* 2003, 3, 1057–1062.
[18] Schabes-Retchkiman P, Canizal G, Herrera-Becerra R, Zorrilla C, Liu H, Ascencio J. *Opt. Mater.* 2006, 29, 95–99.
[19] Ismail M, Gul S, Khan MI, Khan MA, Asiri AM, Khan SB. *Green Process. Synth.* 2019, 8, 135–143.
[20] Khan SA, Bello BA, Khan JA, Anwar Y, Mirza MB, Qadri F, Farooq A, Adam IK, Asiri AM, Khan SB. *J. Photochem. Photobiol. B* 2018, 1, 62–70.

[21] Singh D, Rathod V, Ninganagouda S, Hiremath J, Singh AK, Mathew J. *Bioinorg. Chem. Appl.* 2014, 2014, 1–8.
[22] Davies RL, Etris SF. *Catal. Today* 1997, 36, 107–114.
[23] Feng QL, Wu J, Chen G, Cui F, Kim T, Kim J. *J. Biomed. Mater. Res.* 2000, 52, 662–668.
[24] Sondi I, Salopek-Sondi B. *J. Colloid Interface Sci*. 2004, 275, 177–182.
[25] Alt V, Bechert T, Steinrücke P, Wagener M, Seidel P, Dingeldein E, Domann E, Schnettler R. *Biomaterials* 2004, 25, 4383–4391.
[26] Choi O, Deng KK, Kim N-J, Ross Jr L, Surampalli RY, Hu Z. *Water Res*. 2008, 42, 3066–3074.
[27] Njagi EC, Huang H, Stafford L, Genuino H, Galindo HM, Collins JB, Hoag GE, Suib SL. *Langmuir* 2010, 27, 264–271.
[28] Ali Khan S, Bahadar Khan S, Kamal T, M Asiri A, Akhtar K. *Recent Pat. Nanotechnol*. 2016, 10, 181–188.
[29] Ismail M, Khan MI, Khan SB, Akhtar K, Khan MA, Asiri AM. *J. Mol. Liq.* 2018, 268, 87–101.
[30] El Gaini L, Lakraimi M, Sebbar E, Meghea A, Bakasse M. *J. Hazard. Mat.* 2009, 161, 627–632.
[31] Ahmed S, Kamal T, Khan SA, Anwar Y, T Saeed M, Muhammad Asiri A, Bahadar Khan S. *Curr. Nanosci.* 2016, 12, 569–575.
[32] Fu F, Dionysiou DD, Liu H. *J. Hazard. Mater.* 2014, 267, 194–205.
[33] Padhi B. *Int. J. Environ. Sci.* 2012, 3, 940.
[34] Wang C, Yediler A, Lienert D, Wang Z, Kettrup A. *Chemosphere* 2002, 46, 339–344.
[35] Weber EJ, Adams RL. *Environ. Sci. Technol.* 1995, 29, 1163–1170.
[36] Ayed L, Mahdhi A, Cheref A, Bakhrouf A. *Desalination* 2011, 274, 272–277.
[37] Anusuya S, Sathiyabama M. *Int. J. Biol. Macromol.* 2015, 77, 9–14.
[38] Roy K, Sarkar CK, Ghosh CK. *Green Process. Synth.* 2015, 4, 455–461.
[39] Maham M, Nasrollahzadeh M, Sajadi SM, Nekoei M. *J. Colloid Interface Sci.* 2017, 497, 33–42.
[40] Agasti N, Kaushik N. *A. J. Nanomater*. 2014, 2, 4–7.
[41] Ishizaki T, Yatsugi K, Akedo K. *Nanomaterials* 2016, 6, 172.
[42] Ismail M, Khan MI, Akhtar K, Khan MA, Asiri AM, Khan SB. *Phys. E (Amsterdam, Neth.)* 2018, 103, 367–376.
[43] Hatamifard A, Nasrollahzadeh M, Sajadi SM. *New J. Chem.* 2016, 40, 2501–2513.
[44] Atarod M, Nasrollahzadeh M, Mohammad Sajadi S. *J. Colloid Interface Sci.* 2016, 462, 272–279.
[45] Naraginti S, Stephen FB, Radhakrishnan A, Sivakumar A. *Spectrochim. Acta A* 2015, 135, 814–819.
[46] Brown GT, Darwent JR. *J.C.S. Faraday 1* 1984, 80, 1631–1643.
[47] Lichter JA, Van Vliet KJ, Rubner MF. *Macromolecules* 2009, 42, 8573–8586.